ACS SENSORS

pubs.acs.org/acssensors

Article

DNA Nanosieve-Based Regenerative Electrochemical Biosensor Utilizing Nucleic Acid Flexibility for Accurate Allele Typing in Clinical Samples

Jin-Yuan Chen,[⊥] Liang-Yong Yang,[⊥] Zhou-Jie Liu, Qing-Xia Wei, Ying Zhang, Bing Wu, Guang-Xian Zhong, Leng-Xi Fu, Xin-Hua Lin,* Xiu-Hua Weng,* and Xiong-Wei Xu*

Cite This: *ACS Sens.* 2021, 6, 1348−1356

Read Online

ACCESS | Metrics & More | Article Recommendations | Supporting Information

ABSTRACT: Herein, an interface-based DNA nanosieve that has the ability to differentiate ssDNA from dsDNA has been demonstrated for the first time. The DNA nanosieve could be readily built through thiol-DNA's self-assembly on the gold electrode surface, and its cavity size was tunable by varying the concentration of thiol-DNAs. Electrochemical chronocoulometry using $[Ru(NH_3)_6]^{3+}$ as redox revealed that the average probe-to-probe separation in the 1 μM thiol-DNA-modified gold electrode was 10.6 ± 0.3 nm so that the rigid dsDNA with a length of ∼17 nm could not permeate the nanosieve, whereas the randomly coiled ssDNA could enter it due to its high flexibility, which has been demonstrated by square wave voltammetry and methylene blue labels through an upside-down hybridization format. After combining the transiently binding characteristic of a short DNA duplex and introducing a regenerative probe (the counterpart of ssDNA), a highly reproducible nanosieve-based E-DNA model was obtained with a relative standard deviation (RSD) as low as 2.7% over seven cycles. Finally, we built a regenerative nanosieve-based E-DNA sensor using a ligation cycle reaction as an ssDNA amplification strategy and realized one-sensor-based continuous measurement to multiple clinical samples with excellent allele-typing performance. This work holds great potential in low-cost and high-throughput analysis between biosensors and biochips and also opens up a new avenue in nucleic acid flexibility-based DNA materials for future applications in DNA origami and molecular logic gates.

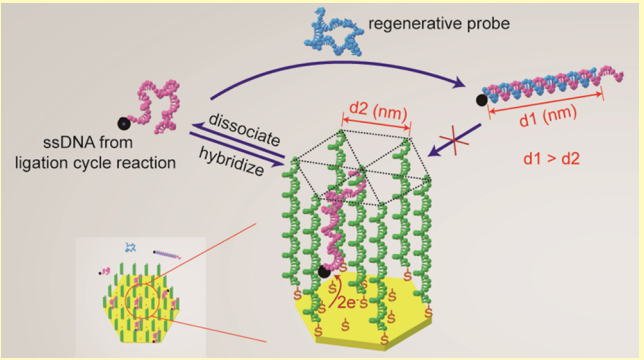

KEYWORDS: *electrochemical DNA sensor, regenerative biosensor, allele typing, DNA nanotechnology, clinical sample*

Electrochemical DNA (E-DNA) sensors, owing to their high sensitivity, low cost and adaptability to point-of-care testing (POCT), have attracted enormous interest in disease diagnosis, environmental monitoring, and food safety for decades.[1,2] These unique properties, however, are fairly compromised by their poor reproducibility due to the large sensor-to-sensor variance resulted from differences in the substrate and modification of each sensor.[3] To address this issue, a sensor regeneration strategy would be a good alternative because it could enable the individual sensor to perform multiple detection methods tautologically so that sensor-to-sensor variance could be eliminated drastically.[4]

To achieve E-DNA sensors' regeneration, the cut-in spot of current strategies is focused on the way how to disrupt hydrogen bonds of a DNA duplex. Therefore, methods including changing the pH value,[5] enhancing the temperature,[6] and adding chemical agents such as guanidine chloride,[7] urea,[8] or glycine[9] are usually employed. Nevertheless, challenging the sensors with these chemical reagents would not only perturb the species and distribution of ions on the sensor interface but also irreversibly destroy the secondary structure of the DNA probes, leading to the change of the DNA self-assembly monolayer (SAM) both in charge and conformation. In this regard, this regeneration process will not be continuous and reliable. Consequently, it is desperately needed, from another perspective, to develop renewable E-DNA sensors with high robustness and reliability.

Typically, the preparation of E-DNA sensors for DNA detection includes the DNA SAM's formation on an electrode surface, the non-covalent hybridization with labeled probes via target-induced sandwich architecture, and the monitoring of electron transfer using the electrochemistry technique. In the

Received: December 30, 2020
Accepted: February 23, 2021
Published: March 4, 2021

https://dx.doi.org/10.1021/acssensors.0c02720
ACS Sens. 2021, 6, 1348−1356

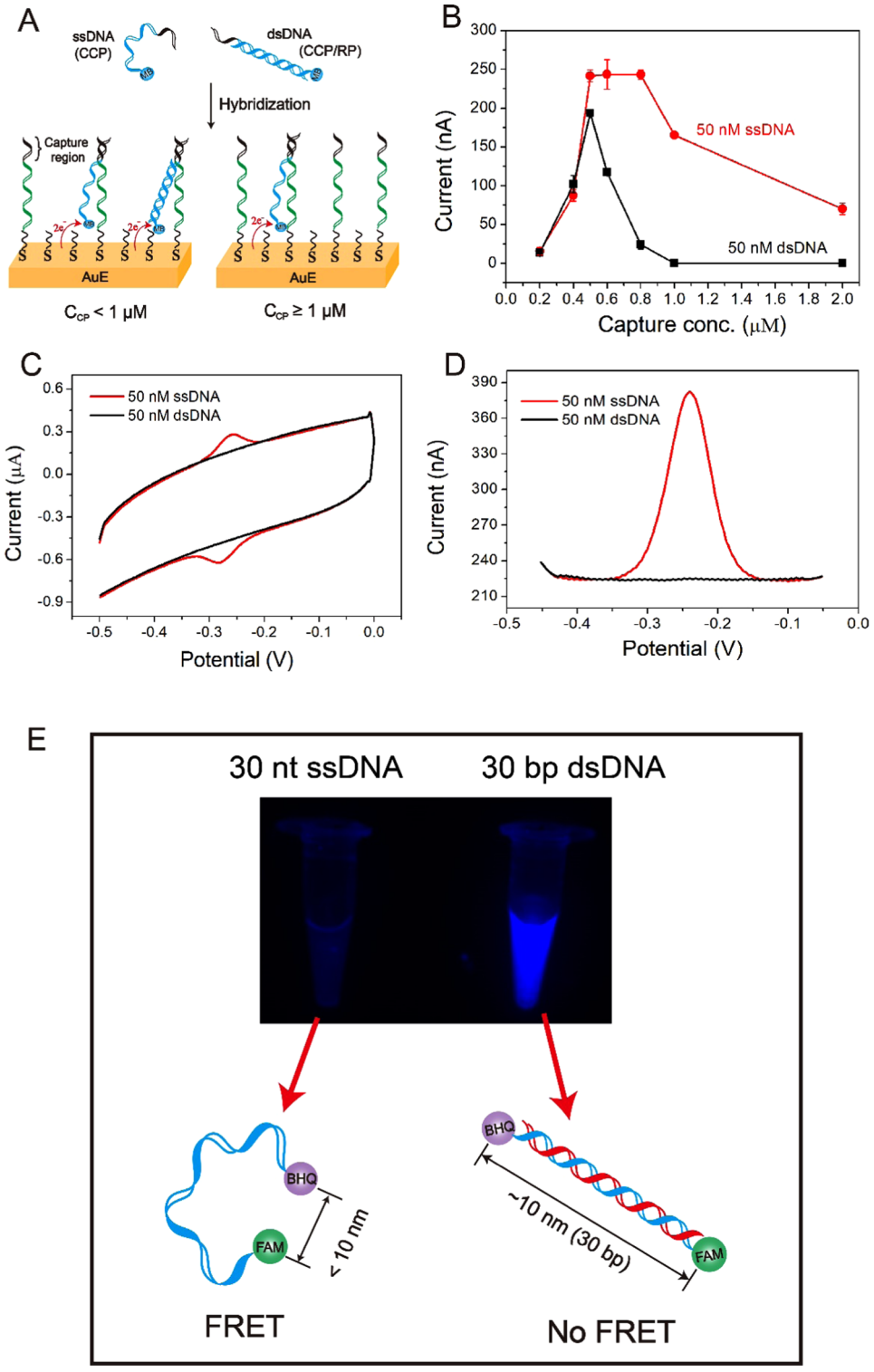

Figure 1. Different accessibilities of ssDNA and dsDNA toward the thiol-DNA SAM using an upside-down hybridization format. (A) Sensor architecture of the upside-down hybridization format with ssDNA and dsDNA. (B) Plots of the SWV current as a function of the concentration of CP in the detection of 50 nM ssDNA and 50 nM dsDNA. Error bars show the standard deviations of measurements taken from three independent experiments (n = 3). (C) Cyclic voltammograms of the 1 μM CP-modified gold electrode after incubation with 50 nM ssDNA and 50 nM dsDNA. (D) SWV curves of the 1 μM CP-modified gold electrode after incubation with 50 nM ssDNA and 50 nM dsDNA. (E) Investigation of the different flexibilities between ssDNA and dsDNA using the FRET method. The concentration of ssDNA was 50 nM in LCR buffer. To form dsDNA, ssDNA and its complementary DNA (red strand) were mixed in LCR buffer with final concentrations of 50 and 200 nM, respectively. Then, the mixed solution was incubated at room temperature for 1 h.

signal-on case, the sandwich-type hybridization with the upside-down format is commonly required to drive the label such as methylene blue (MB) and ferrocene (Fc) in close proximity to the electrode surface.[10,11] It is worth noting that

https://dx.doi.org/10.1021/acssensors.0c02720
ACS Sens. 2021, 6, 1348−1356

the course of sandwich-type hybridization with the upside-down format is quite different from that with the upright format commonly used in enzyme-catalyzed E-DNA sensors.[12] For the latter, only the protruding ssDNA is needed to enter into the SAM and accomplish the hybridization; however, the former requires the dsDNA part to permeate the SAM, so that the protruded ssDNA can adequately collide with the capture probe to form sandwich architecture.[13−15] To our knowledge, ssDNA is coiled and flexible, whereas dsDNA is characteristic of a rigid structure; this flexibility difference between ssDNA and dsDNA has been commonly recognized and widely exploited to construct electrochemical biosensors.[16,17] In the present study, their different flexibilities have been experimentally verified using the fluorescence resonance energy transfer (FRET) method, showing significantly different accessibilities to the SAM.

Inspired by such a difference in accessibility to the SAM between ssDNA and dsDNA, we herein, for the first time, propose a novel regenerative E-DNA sensor through concentration-dependent DNA self-assembly, forming a nanosieve with the ability to differentiate ssDNA from dsDNA. We assume that the stick-like dsDNA, due to its longer length than the cavity size of the nanosieve, would be obstructed away from the nanosieve and fail to hybridize with the capture probe in the upside-down format. Conversely, the coiled ssDNA can easily permeate through the nanosieve and complete hybridization for its high flexibility. Previously, it has been widely reported that hybridization of short oligonucleotides (8−12 bp) consists of a dynamic equilibrium process of binding and dissociation, which has been demonstrated by a total internal reflection fluorescence microscope.[18−20] As such, when the nanosieve-based E-DNA sensor is proposed to detect ssDNA, the complementary DNA, which we named regenerative probe (RP), can be added to break the equilibrium process of ssDNA, as the formed dsDNA would be obstructed in the mouth of the nanosieve, resulting in the removal of the ssDNA from the SAM and the disappearance of the electrical signal. In this way, the nanosieve-based E-DNA sensor can be readily regenerated for the next round of testing without disrupting the DNA SAM. This study, coupling the flexibility difference between ssDNA and dsDNA with the transiently binding characteristic of a short DNA duplex, offers a new regeneration strategy based on a cavity-tunable nanochannel for hybridization and the employment of RP, opening up a new avenue for applications of E-DNA sensors with greatly improved reproducibility and significantly lower cost.

EXPERIMENTAL SECTION

Reagents and Materials. Tris(2-carboxyethyl) phosphine hydrochloride (TCEP), 6-mercapto-1-hexanol (MCH), and hexaammineruthenium(III) chloride ($[Ru(NH_3)_6]^{3+}$) were purchased from Sigma-Aldrich. Thermal stable ampligase and 10× reaction buffer (pH 8.3) containing 200 mM Tris-HCl, 250 mM KCl, 100 mM $MgCl_2$, 5 mM NAD, and 0.1% Triton X-100 were purchased from Epicenter Technologies (Madison). Al_2O_3 alumina slurry (0.05 μm) was purchased from Chenhua Instrument Co., Ltd. (Shanghai, China). DNA strands used in this work were high-performance liquid chromatography (HPLC) purified and synthesized by TAKARA. The sequences of various strands used in this work are shown in Table S1. Unless otherwise indicated, all other reagents and solvents purchased were of analytical grade and used without further purification.

The buffers and solutions involved in this work were as follows: DNA immobilization buffer (10 mM Tris-HCl + 1 mM ethylenediaminetetraacetic acid (EDTA) + 1 M NaCl + 10 mM TCEP, pH 7.4), DNA hybridization buffer, ligation cycle reaction (LCR) buffer (1× reaction buffer), and detection buffer (phosphate buffered saline (PBS), 10 mM PB + 1 M NaCl, pH 7.4).

Preparation of the Nanosieve-Based E-DNA Sensor. Gold electrodes (2 mm in diameter) were mechanically polished and electrochemically cleaned prior to all experiments. The gold electrodes were polished using a 0.05 μm Al_2O_3 suspension on chamois leather, with sonication in ethanol or water after each step. Subsequently, electrochemical scanning was performed using cyclic voltammetry in H_2SO_4 (0.5 M, 0−1.6 V vs Ag/AgCl/3 M KCl, 100 mV/s) until stable voltammograms were obtained. The electrodes were rinsed with deionized water and dried under N_2 flow for further modification.

The capture probe stock solution (100 μM) was diluted to 1 μM using DNA immobilization buffer. Then, 3 μL volume of this solution was dropped onto the cleaned electrode surface for 16 h to form a thiol-DNA self-assembly monolayer (SAM). Afterward, it was rinsed with 10 mM PB buffer and incubated in 2 mM MCH in deionized water for another 2 h to displace non-specifically adsorbed DNA and passivate the remaining electrode area.

Electrochemical Measurements. Electrochemical measurements were performed at room temperature (25 °C) on an electrochemical workstation (CHI 760d; CH Instruments, Austin, TX) using a standard three-electrode cell containing a Au-disk working electrode (2 mm diameter), a Ag/AgCl reference electrode, and a Pt wire auxiliary electrode. The interrogate of the MB signal employed square wave voltammetry (SWV, from −0.5 to −0.05 V in an increment of 0.004 V vs Ag/AgCl, with an amplitude of 25 mV and a frequency of 100 Hz) and cyclic voltammetry (CV, from −0.5 to −0.05 V in 0.1 V/s with a sample interval of 1 mV) in PBS.

RESULTS AND DISCUSSION

Study on the Different Accessibilities of ssDNA and dsDNA Toward the Thiol-DNA SAM Using the Upside-Down Hybridization Format. To the best of our knowledge, the different accessibilities of ssDNA and dsDNA toward the thiol-DNA SAM using the upside-down hybridization format have not been explored until now (see Figure 1A). Herein, we vividly call the thiol-DNA SAM as a nanosieve, as shown in Table of Content (TOC) from a three-dimensional angle, which has the ability to distinguish ssDNA and dsDNA by tuning its cavity size at the nanoscale via packing different concentrations of thiol-DNAs on the surface of the gold electrode. As a proof of concept, two model targets were employed. One is a synthetic ssDNA (CCP), which is 12 nt complementary to the capture probe (CP) on its 5′ end and labeled with an MB redox on its 3′ end, and the other is a partial dsDNA (51 bp duplex between CCP and RP). Electrochemical signals from MB can be quantitatively detected using the square wave voltammetry (SWV) technique only when these two model targets penetrate the nanosieve to hybridize with CP and make the MB label tether to the electrode surface.

As shown in Figure 1B, the current response from dsDNA decreased more obviously than that of ssDNA as the concentration of CP increased from 0.5 to 1 μM, which demonstrated the enhanced difficulty for dsDNA to permeate the thiol-DNA SAM when the spacing between CPs got narrower. In other words, the subtle change in the cavity size of the nanosieve significantly affected the entry of dsDNA into the SAM, but not for ssDNA, although they have the same length in geometry. Probing into the difference between dsDNA and ssDNA, it is found that the biggest change is their flexibility: the duplex hybrid endows itself with an enhanced rigid structure, while the ssDNA is coiled like a ball of wool. The stick-like dsDNA, due to its enhanced electrostatic

https://dx.doi.org/10.1021/acssensors.0c02720
ACS Sens. 2021, 6, 1348−1356

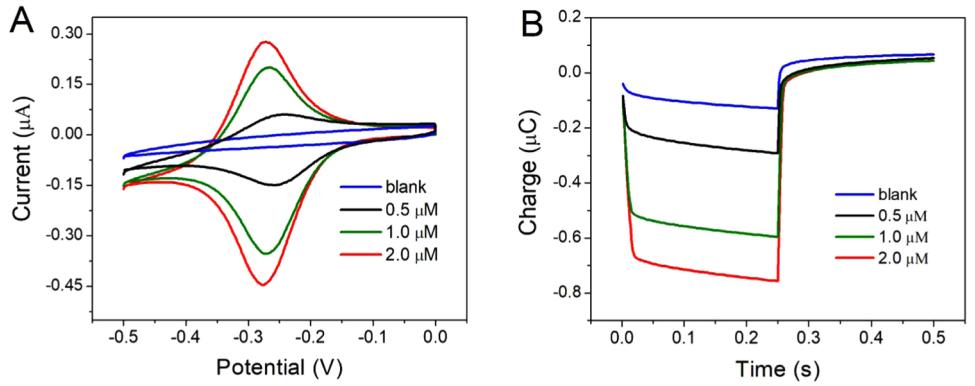

Figure 2. Cyclic voltammograms (A) and chronocoulometry curves (B) of gold electrodes modified with 0.5, 1, and 2 μM CP in 10 mM Tris-HCl buffer (pH = 7.4) after incubation with 50 μM $[Ru(NH_3)_6]^{3+}$. The blank was obtained via measuring the CP-modified gold electrode in Tris-HCl buffer without $[Ru(NH_3)_6]^{3+}$, representing the amount of the charge in the double layer of the electrode interface.

repulsion as the exposed PO_4^- group increased significantly, is compelled to enter the nanosieve in a lateral way but not in a vertical direction so that the dsDNA is not vertically inserted into the sieve, and therefore the length of dsDNA plays a decisive role in its permeation into the nanosieve, which makes it easy to get stuck in the cavity when it approaches a cavity with a smaller diameter. For ssDNA, its high flexibility endows it with variable shapes, which means that it is not merely constrained by its size when passing into the nanosieve and can adapt to the nanosieve by making changes, wriggling just like a worm. As shown in Figure 1C,D, there was no electrochemical signal for dsDNA when the concentration of CP reached 1 μM; however, ssDNA could generate a strong electrochemical signal even in the circumstance of 2 μM CP, as indicated in Figure 1B.

To further confirm this event, we experimentally verified the flexibility difference between ssDNA and dsDNA using the FRET method. As we know, FRET is a nonradiative energy transfer process that occurs when a donor (such as FAM) and an acceptor (such as BHQ) are within a distance of 10 nm. Herein, a 30 bp dsDNA model with a geometrical length of ~10.2 nm was employed. As shown in Figure 1E, the ssDNA with FAM and BHQ modification on its 5′ and 3′ terminals showed no visible fluorescence under blue excitation light (left). However, there was a strong fluorescence after the complementary DNA was added to form dsDNA (right). This result demonstrated that the ssDNA presented a coiled state so that the FAM was in proximity to the BHQ (<10 nm), resulting in the fluorescence quenching of FAM, while the ssDNA should be completely straightened (~10.2 nm) after the addition of the complementary DNA, forming a rigid structure to ensure that the distance between the FAM and the BHQ was over 10 nm so that the fluorescence was recovered. Altogether, the previous reports[16,17] combined with the results using the FRET method prove the flexibility difference between ssDNA and dsDNA (coiled for ssDNA and rigid for dsDNA).

Quantification of the Thiol-DNA Density on the Gold Electrode Surface. Based on the abovementioned results, it can be concluded that the nanosieve with a proper cavity size had the ability to achieve differentiation between ssDNA and dsDNA, in which the cavity size is hypothetically considered to be smaller than the length of dsDNA, and this size is tunable at the nanoscale by varying the different concentrations of CP. Clearly, the dsDNA part (51 bp) between CCP and RP in this study has a length of 17 nm. As such, the cavity size of the nanosieve, that is, the average spacing of the CP needs to be determined to support the aforesaid mechanism. To do this, simple and rapid cyclic voltammetry and chronocoulometry based on the quantitation of electrostatically bound redox cations ($[Ru(NH_3)_6]^{3+}$) were used.[21] This method has been widely employed for determining the surface density of DNA strands immobilized on the electrode surface with the assumption that the negative charges on DNA phosphate backbones are combined with multiple-charged $[Ru(NH_3)_6]^{3+}$ cations. As shown in Figure 2, the cathodic peak of $[Ru(NH_3)_6]^{3+}$ increased with the increasing concentration of thiol-DNA from 0 to 2 μM, suggesting the increasing amount of thiol-DNAs on the electrode surface via the Au−S bond and the decreased average probe-to-probe separation.

Especially, the number of DNA strands per unit area (Γ_{DNA}) immobilized on an electrode and the average probe-to-probe separation were calculated using the previously reported method[13] (details shown in the Supporting Information). In the case of 1 μM thiol-DNA, the probe-to-probe separation or the cavity size of the nanosieve was calculated to be 10.6 nm (seeing Table 1), which was smaller than the length of the employed dsDNA (17 nm), while a 21.3 nm cavity nanosieve was obtained when employing 0.5 μM thiol-DNA, in which both ssDNA and dsDNA can permeate this nanosieve and produce an electrochemical signal. Hence, the determined results by electrochemistry preliminarily validated our hypothesis.

Table 1. Characterization of the Thiol-DNA Density on the Gold Electrode

thiol-DNA concentration (μM)	Γ_{DNA} (molecules/cm^2)	average probe-to-probe separation (nm)
0.5	$(2.82 \pm 0.01) \times 10^{11}$	21.3 ± 0.5
1.0	$(1.13 \pm 0.06) \times 10^{12}$	10.6 ± 0.3
2.0	$(1.41 \pm 0.02) \times 10^{12}$	9.5 ± 0.1

Regeneration Mechanism of the Nanosieve-Based E-DNA Sensor. Based on the aforementioned results and demonstrations, a new regeneration mechanism was therefore proposed by combining the dynamic hybridization characteristic of short oligonucleotides. The hypothetic process was as follows: a Au electrode packed with a 10.6 nm cavity nanosieve was challenged to CCP with a dynamic hybridization process and produced an MB signal (signal-on), and then the added

https://dx.doi.org/10.1021/acssensors.0c02720
ACS Sens. 2021, 6, 1348−1356

RP was prompted to form stick-like dsDNA when the CCP was free to the homogeneous solution, due to the fact that the homogeneous environment better facilitates hybridization than the heterozygous surface (as shown in Figure S1). Finally, the dsDNA was obstructed by the nanosieve, owning to its longer length, leading to the absolute disappearance of the MB signal (signal-off). In this way, the nanosieve-based E-DNA sensor can be readily regenerated for the next detection without using any destructive reagents and changing the state of the SAM. Of note, it must be confirmed that the broken equilibrium process was solely caused by the complementary DNA (RP) and not by dilution buffer or uncomplementary DNA, so experiments proving the unique role of RP were performed: the nanosieve was generated via self-assembly of 1 μM thiol-DNAs on the gold electrode, and then 50 nM CCP was used to challenge it and produced a strong MB signal. As shown in Figure 3c, when

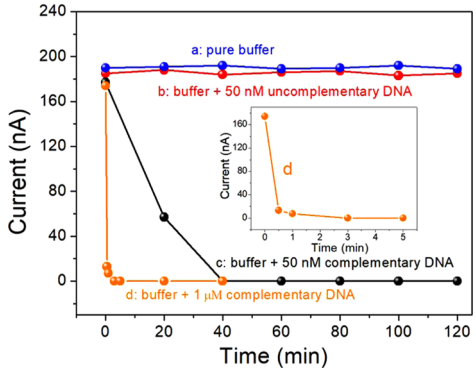

Figure 3. Plots of the SWV current response from the nanosieve-based E-DNA sensor built through 1 μM CP after incubation with (a) pure buffer: 10 mM phosphate buffer + 1 M NaCl, (b) buffer containing 50 nM uncomplementary DNA, (c) buffer containing 50 nM complementary DNA, and (d) buffer containing 1 μM complementary DNA as a function of time (the inset shows the kinetic curve of (d) within 5 min).

50 nM RP complementary to CCP was introduced, such a current signal decreased and leveled off to zero absolutely as time extended to 40 min, while there were no obvious changes in the current response when we challenged the sensor with pure buffer (curve a) or buffer containing uncomplementary DNA (curve b), thus illustrating the unique role of RP in breaking the equilibrium process of CCP. Surprisingly, the employment of 1 μM RP decreased the current sharply, disappearing within 3 min (Figure 3d), indicating that higher RP enabled a high collision frequency between the dissociative state of CCP and RP and fast hybridization dynamics so that very fast regeneration could be obtained. In addition, when the sensor was packed with the nanosieve generated via 500 nM thiol-DNAs, there was only a slow and slight signal depression under the same experiment condition (Figure S2), indicating the importance of the concentration of CP that was required to construct a nanosieve with a proper cavity size to selectively accommodate DNAs with different morphologies.

Performance of the Regenerative Nanosieve-Based E-DNA Sensor. To judge the regenerative performance of the constructed nanosieve-based E-DNA sensor, the "on-and-off" cycling number was investigated by alternately introducing the CCP and RP, in which SWV was performed after each incubation. As presented in Figure 4, the SWV response was completely eliminated in each cycle when adding the RP and

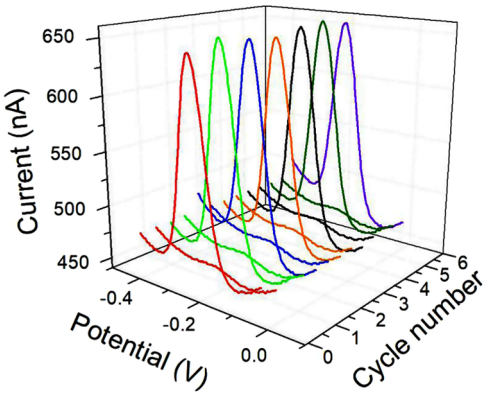

Figure 4. SWV response of the regenerative nanosieve-based E-DNA sensor built through 1 μM CP toward 50 nM CCP and after challenging with 1 μM RP over seven cycles.

recovered again after the addition of CCP, which suggested the high regeneration efficiency of this nanosieve. Notably, the recovered SWV response was stable enough with a relative standard deviation (RSD) as low as 2.7% over seven cycles, which was superior to other regenerative biosensors. This result indicated that the regenerative nanosieve-based E-DNA sensor had high accuracy that was essential to conduct continuous detection toward different samples, and this could be ascribed to the self-cleaning function of the involved RP without disrupting the surface's SAM, which held great advantages for expanding the application of E-DNA sensors in clinical diagnosis.

Design and Optimization of the *CYP2C19*2* Genotyping Method Using the Regenerative Nanosieve-Based E-DNA Sensor. Based on the proposed regenerative nanosieve-based E-DNA sensor, we here first exploited its application in allele typing using a ligation cycle reaction (LCR) as an amplification strategy,[22] in which the lengthened ssDNA from the LCR can hybridize with the CP in the nanosieve layer and produce the MB signal. Herein, *CYP2C19*, an important human drug metabolism gene responsible for metabolizing commonly used drugs including clopidogrel, proton pump inhibitors (PPIs), etc.,[23] was chosen as the detection target. *CYP2C19*1* is a wild-type allele that encodes an enzyme for its normal activity, whereas *CYP2C19*2*, an important mutant site in the *CYP2C19* gene occurring at G681A, encodes an inactive enzyme, resulting in poor metabolism, and *CYP2C19*1*2* is a heterozygous allele encoding a medium-activity enzyme. Troublesomely, G−T can form wobble pairs with two hydrogen bonds in diverse contexts, the stability of which is comparable with that of the A−T perfect pair.[24] Thus, distinguishing these three types imposes a great challenge and plays a critical role in predicting the risk of drug metabolism as well as in the individualized drug therapy of clinical practice.

As shown in Scheme 1, the 5′ end of the auxiliary probe (AP) has 12 bases pairing with the CP in the nanosieve layer, and the signal probe (SP) with a PO_4 group on its 3′ end was labeled with an MB at the terminal T base. These two probes can be ligated by the mutation recognizing ligase-ampligase in the presence of target DNA, whereas this event could be inhibited when there is a mismatched base in the ligation site. Considering that the unligated AP can also hybridize with the CP and the length of the AP/RP duplex is shorter than the cavity size of the DNA SAM, which will lead to the failure of

https://dx.doi.org/10.1021/acssensors.0c02720
ACS Sens. 2021, 6, 1348−1356

Scheme 1. Schematic Illustration of the Regenerative Nanosieve-Based E-DNA Sensor Using Ligation Cycle Reaction Amplification

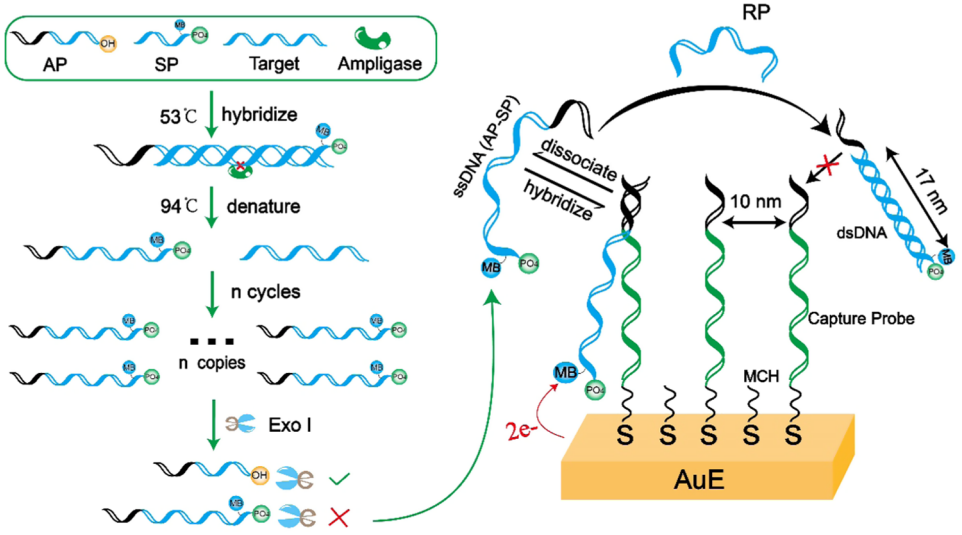

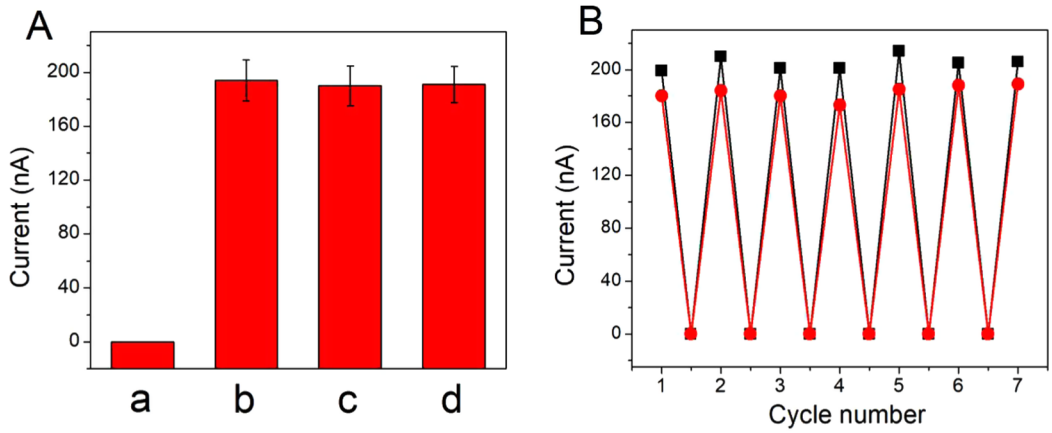

Figure 5. (A) SWV response from (a) 10 ng/μL salmon sperm genome DNA, (b) 5 nM synthetic target DNA, (c) 5 ng/μL salmon sperm genome DNA spiked with 5 nM synthetic target DNA, and (d) 10 ng/μL salmon sperm genome DNA spiked with 5 nM synthetic target DNA. Mean values and standard deviations were obtained from three independent experiments. (B) Graph for the regeneration of the nanosieve-based E-DNA sensor toward 5 nM synthetic target DNA (black) and 10 ng/μL salmon sperm DNA spiked with 5 nM synthetic target DNA (red) when challenged with 1 μM RP.

dissociation of AP from the electrode. As the report goes, Exonuclease I (Exo I) could digest ssDNA in the direction 3′ → 5′ and show no activity toward ssDNA with 3′-modification.[25] Exactly, our agarose electrophoresis experiment (Figure S4) demonstrated that the digestion of Exo I was inhibited dramatically toward the ssDNA with 3′-PO_4. Therefore, Exo I could be employed to digest the unligated AP from its 3′-OH after the LCR, while the ligated AP−SP can be protected from digestion due to its 3′-PO_4. Under optimized conditions, this proposed regenerative nanosieve-based E-DNA sensor exhibited high selectivity toward the synthetic target with a linear range of 0.1−5 nM and a limit of detection of 100 pM (Figure S5). On the contrary, there was a weak current response obtained from the synthetic target with a single-base mismatch (Figure S6).

As is well-known, there are a variety of components in real samples, such as nucleic acid extract, which may affect the amplification efficiency of LCR and lower the regeneration performance of the E-DNA sensor. Therefore, it is needed to perform anti-interference analysis by mixing the target DNA with salmon sperm genome DNA that is similar to the human genome DNA and generally used as the simulated sample. Usually, the concentration of extracted genomic DNA from human whole blood using a commercial kit was from 10 to 100 ng/μL, so 10 μL volume of salmon sperm genome DNA (50 and 100 ng/μL) was chosen to be added into a 90 μL LCR reaction system with final concentrations of 5 and 10 ng/μL. As obtained in Figure 5A, the addition of salmon sperm genome DNA did not attenuate the current response from the synthetic target DNA even at 100 ng/μL. Also, to investigate the interference of genome DNA on the proposed regeneration process, regeneration cycles in the circumstance of synthetic target DNA added with salmon sperm genome DNA were performed to compare with that of only synthetic target DNA. As shown in Figure 5B, both of them showed reproducible on-and-off cycling, which demonstrated the excellent anti-interference capability of the proposed generative nanosieve-based E-DNA sensor. For this excellent performance, it could be ascribed to the impressive obstruction of the nanosieve and the effective removal of unwanted DNA probes' adsorption via

https://dx.doi.org/10.1021/acssensors.0c02720
ACS Sens. 2021, 6, 1348−1356

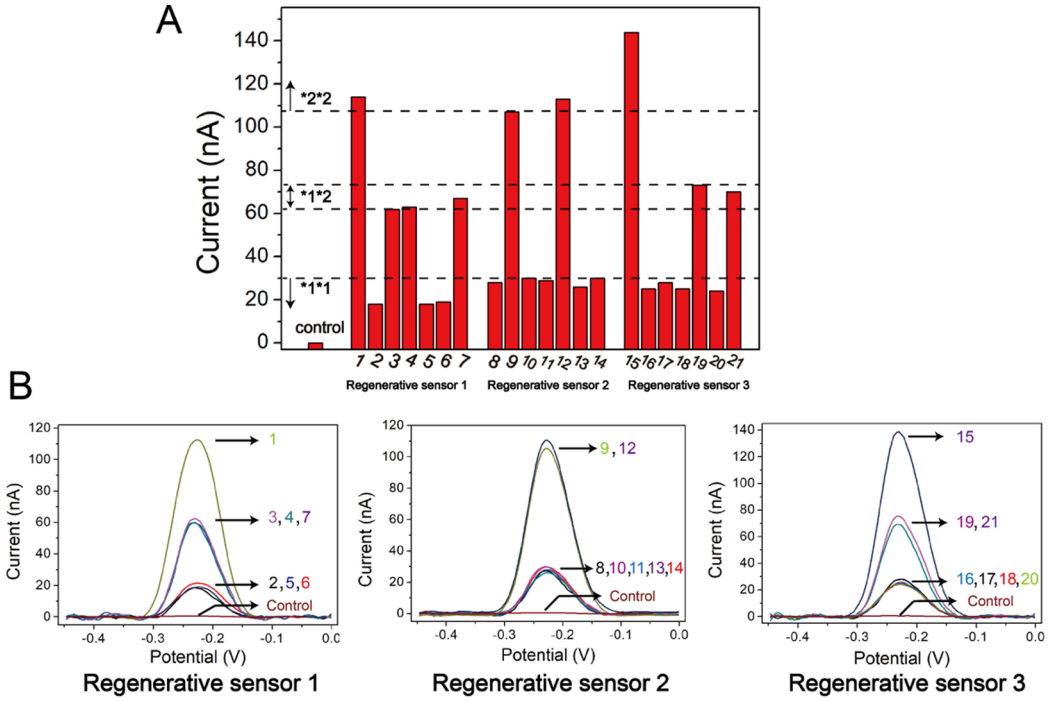

Figure 6. SWV responses (A) and square wave voltammograms (B) of the three independent regenerative nanosieve-based E-DNA sensors when used to analyze clinical samples with salmon sperm genome DNA as control.

phosphate buffer regulation,[26] which ensured that the nanosieve is neat and tidy for each regeneration cycle.

Application in the Clinical Sample. As proved to have a high anti-interference ability in the simulated sample, we further examined its real-sample assay in clinical practice. To demonstrate this, a double-blind experiment was performed. Twenty-one cases of human whole blood samples were collected from the Department of Pharmacy of the First Affiliated Hospital of Fujian Medical University. After extracting the total nucleic acid and conducting the polymerase chain reaction (PCR), the LCR was carried out and measured using the proposed regenerative nanosieve-based E-DNA sensor. Therein, each sensor measured seven different samples successively after each regeneration. As shown in Figure 6, SWV current responses were significantly distributed in three regions: 107−144 nA (high), 62−74 nA (medium), and 18−30 nA (low). Hence, we accordingly determined those samples whose current response fell in the high, medium, and low regions as *CYP2C19*2*, *CYP2C19*1*, and *CYP2C19*1*2* based on the principle of our method. Parallelly, agarose gel electrophoresis (Figure S8A) was performed to confirm the successful PCR amplification of these three types of *CYP2C19* samples. As shown in lane 1 (*CYP2C19*1*), lane 2 (*CYP2C19*2*), and lane 3 (*CYP2C19*1*2*), three bright bands can be observed, indicating the successful PCR of these samples. However, these three bands showing the same brightness (Figure S8B) could not distinguish their genotypes, while current responses obtained from the proposed nanosieve-based E-DNA sensor were quite distinctive. Then, we compared these results determined by the regenerative sensor with the sequencing results of a gold standard method for single nucleotide polymorphism (SNP) detection (Figure S7). Excitingly, these two results in genotyping of *CYP2C19* were fully matched, which confirmed the high accuracy of the regenerative nanosieve-based E-DNA sensor in continuously measuring multiple samples, exhibiting the excellent allele-typing ability of the regenerative nanosieve-based E-DNA sensor and its huge potential in low-cost and high-throughput analysis in SNP-related diseases.

CONCLUSIONS

In summary, we developed a new regenerative E-DNA sensor from the point of view of probe regulation without the employment of destructive reagents. Specifically, a DNA nanosieve that has the ability to differentiate ssDNA from dsDNA has been demonstrated in this study for the first time. Taking advantage of the transiently binding characteristic of a short DNA duplex, a highly reproducible nanosieve-based E-DNA model was successfully constructed. Consequently, we built the regenerative nanosieve-based E-DNA sensor using a ligation cycle reaction as an ssDNA amplification strategy and realized one-sensor-based continuous measurement to multiple clinical samples with excellent allele-typing performance. This work provided a new perspective based on the probe-regulation strategy to develop regenerative biosensors and gave us a hint that the flexibility difference between ssDNA and dsDNA endows them with different physicochemical properties, which could be useful in the design of DNA-based sensors and materials.

ASSOCIATED CONTENT

Supporting Information

The Supporting Information is available free of charge at https://pubs.acs.org/doi/10.1021/acssensors.0c02720.

Supporting protocol for experiments; DNA sequences used in this study; and supporting figures (PDF)

AUTHOR INFORMATION

Corresponding Authors

Xin-Hua Lin − *Department of Pharmaceutical Analysis, Higher Educational Key Laboratory for Nano Biomedical*

https://dx.doi.org/10.1021/acssensors.0c02720
ACS Sens. 2021, 6, 1348−1356

Technology of Fujian Province, Faculty of Pharmacy, Fujian Medical University, Fuzhou 350122, China; Email: xhl1963@sina.com

Xiu-Hua Weng − *Department of Pharmacy, The First Affiliated Hospital, Fujian Medical University, Fuzhou 350005, China*; Email: shirly0409@163.com

Xiong-Wei Xu − *Department of Pharmacy, The First Affiliated Hospital, Fujian Medical University, Fuzhou 350005, China*; orcid.org/0000-0002-4787-2506; Email: xxw0409@163.com

Authors

Jin-Yuan Chen − *The Central Laboratory, Fujian Key Laboratory of Precision Medicine for Cancer, The First Affiliated Hospital, Fujian Medical University, Fuzhou 350005, China; Key Laboratory of Radiation Biology of Fujian Higher Education Institutions, The First Affiliated Hospital, Fujian Medical University, Fuzhou 350005, China*; orcid.org/0000-0002-0355-9892

Liang-Yong Yang − *Department of Pharmacy, The First Affiliated Hospital, Fujian Medical University, Fuzhou 350005, China*

Zhou-Jie Liu − *Department of Pharmacy, The First Affiliated Hospital, Fujian Medical University, Fuzhou 350005, China*

Qing-Xia Wei − *Department of Pharmacy, The First Affiliated Hospital, Fujian Medical University, Fuzhou 350005, China*

Ying Zhang − *The Central Laboratory, Fujian Key Laboratory of Precision Medicine for Cancer, The First Affiliated Hospital, Fujian Medical University, Fuzhou 350005, China; Key Laboratory of Radiation Biology of Fujian Higher Education Institutions, The First Affiliated Hospital, Fujian Medical University, Fuzhou 350005, China*

Bing Wu − *The Central Laboratory, Fujian Key Laboratory of Precision Medicine for Cancer, The First Affiliated Hospital, Fujian Medical University, Fuzhou 350005, China; Key Laboratory of Radiation Biology of Fujian Higher Education Institutions, The First Affiliated Hospital, Fujian Medical University, Fuzhou 350005, China*

Guang-Xian Zhong − *The Central Laboratory, Fujian Key Laboratory of Precision Medicine for Cancer, The First Affiliated Hospital, Fujian Medical University, Fuzhou 350005, China; Key Laboratory of Radiation Biology of Fujian Higher Education Institutions, The First Affiliated Hospital, Fujian Medical University, Fuzhou 350005, China*

Leng-Xi Fu − *The Central Laboratory, Fujian Key Laboratory of Precision Medicine for Cancer, The First Affiliated Hospital, Fujian Medical University, Fuzhou 350005, China; Key Laboratory of Radiation Biology of Fujian Higher Education Institutions, The First Affiliated Hospital, Fujian Medical University, Fuzhou 350005, China*

Complete contact information is available at: https://pubs.acs.org/10.1021/acssensors.0c02720

Author Contributions

[⊥]J.-Y.C. and L.-Y.Y. contributed equally to this work.

Notes

The authors declare no competing financial interest.

■ ACKNOWLEDGMENTS

This work was financially supported by the National Natural Science Foundation of China (21904019, 22074017, 81973473, and 81903578), the United Fujian Provincial Health and Education Project for Tackling the Key Research, P. R. China (2019-WJ-11), and the Medical Innovation Project of Fujian Province (2019-CX-24).

■ REFERENCES

(1) Somasundaram, S.; Easley, C. J. A nucleic acid nanostructure built through on-electrode ligation for electrochemical detection of a broad range of analytes. *J. Am. Chem. Soc.* **2019**, *141*, 11721−11726.

(2) Wang, Q.; Wen, Y.; Li, Y.; Liang, W.; Li, W.; Li, Y.; Wu, J.; Zhu, H.; Zhao, K.; Zhang, J.; Jia, N.; Deng, W.; Liu, G. Ultrasensitive electrochemical biosensor of bacterial 16S rRNA gene based on polyA DNA probes. *Anal. Chem.* **2019**, *91*, 9277−9283.

(3) Li, H.; Dauphin-Ducharme, P.; Ortega, G.; Plaxco, K. W. Calibration-free electrochemical biosensors supporting accurate molecular measurements directly in undiluted whole blood. *J. Am. Chem. Soc.* **2017**, *139*, 11207−11213.

(4) Goode, J. A.; Rushworth, J. V.; Millner, P. A. Biosensor regeneration: a review of common techniques and outcomes. *Langmuir* **2015**, *31*, 6267−6276.

(5) Radi, A.-E.; Acero Sánchez, J. L.; Baldrich, E.; O'Sullivan, C. K. Reagentless, Reusable, Ultrasensitive electrochemical molecular beacon aptasensor. *J. Am. Chem. Soc.* **2006**, *128*, 117−124.

(6) Chen, J. Y.; Liu, Z. J.; Zheng, Y. J.; Lin, Z.; Sun, Z. L.; Liu, A. L.; Chen, W.; Lin, X. H. B/C genotyping of hepatitis B virus based on dual-probe electrochemical biosensor. *J. Electroanal. Chem.* **2017**, *785*, 75−79.

(7) Wang, T.; Viennois, E.; Merlin, D.; Wang, G. Microelectrode miRNA sensors enabled by enzymeless electrochemical signal amplification. *Anal. Chem.* **2015**, *87*, 8173−8180.

(8) Wang, L. L.; Wen, Y. L.; Yang, X.; Xu, L.; Liang, W.; Zhu, Y.; Wang, L. H.; Li, Y.; Li, Y.; Ding, M.; Ren, S. Z.; Yang, Z. Z.; Lv, M.; Zhang, J. C.; Ma, K.; Liu, G. Ultrasensitive electrochemical DNA biosensor based on a label-free assembling strategy using a triblock polyA DNA probe. *Anal. Chem.* **2019**, *91*, 16002−16009.

(9) Zeng, G. M.; Zhang, C.; Huang, D. L.; Lai, C.; Tang, L.; Zhou, Y. Y.; Xu, P.; Wang, H.; Qin, L.; Cheng, M. Practical and regenerable electrochemical aptasensor based on nanoporous gold and thymine-Hg^{2+}-thymine base pairs for Hg^{2+} detection. *Biosens. Bioelectron.* **2017**, *90*, 542−548.

(10) Jampasa, S.; Siangproh, W.; Laocharoensuk, R.; Yanatatsaneejit, P.; Vilaivan, T.; Chailapakul, O. A new DNA sensor design for the simultaneous detection of HPV type 16 and 18 DNA. *Sens. Actuators, B* **2018**, *265*, 514−521.

(11) Li, F.; Yu, Z.; Xu, Y.; Ma, H.; Zhang, G.; Song, Y.; Yan, H.; He, X. Using the synergism strategy for highly sensitive and specific electrochemical sensing of streptococcus pneumoniae lyt-1 gene sequence. *Anal. Chim. Acta* **2015**, *886*, 175−181.

(12) Chen, J.; Liu, Z.; Peng, H.; Zheng, Y.; Lin, Z.; Liu, A.; Chen, W.; Lin, X. Electrochemical DNA biosensor based on grafting-to mode of terminal deoxynucleoside transferase-mediated extension. *Biosens. Bioelectron.* **2017**, *98*, 345−349.

(13) Mahshid, S. S.; Camire, S.; Ricci, F.; Vallee-Belisle, A. A highly selective electrochemical DNA-based sensor that employs steric hindrance effects to detect proteins directly in whole blood. *J. Am. Chem. Soc.* **2015**, *137*, 15596−15599.

(14) Mahshid, S. S.; Mahshid, S.; Vallée-Bélisle, A.; Kelley, S. O. Peptide-mediated electrochemical steric hindrance assay for one-step detection of HIV antibodies. *Anal. Chem.* **2019**, *91*, 4943−4947.

(15) Zhou, W.; Mahshid, S. S.; Wang, W.; Vallee-Belisle, A.; Zandstra, P. W.; Sargent, E. H.; Kelley, S. O. Steric hindrance assay for secreted factors in stem cell culture. *ACS Sens.* **2017**, *2*, 495−500.

(16) Hsieh, K.; White, R. J.; Ferguson, B. S.; Plaxco, K. W.; Xiao, Y.; Soh, H. T. Polarity-switching electrochemical sensor for specific detection of single-nucleotide mismatches. *Angew. Chem., Int. Ed.* **2011**, *50*, 11176−11180.

(17) Yang, W.; Lai, R. Y. A dual-signalling electrochemical DNA sensor based on target hybridization-induced change in DNA probe flexibility. *Chem. Commun.* **2012**, *48*, 8703−8705.

(18) Jungmann, R.; Steinhauer, C.; Scheible, M.; Kuzyk, A.; Tinnefeld, P.; Simmel, F. C. Single-molecule kinetics and super-resolution microscopy by fluorescence imaging of transient binding on DNA origami. *Nano Lett.* **2010**, *10*, 4756−4761.
(19) Yu, Y.; Ma, L.; Li, L.; Deng, Y.; Xu, L.; Liu, H.; Xiao, L.; Su, X. Digestion of dynamic substrate by exonuclease reveals high single-mismatch selectivity. *Anal. Chem.* **2018**, *90*, 13655−13662.
(20) Johnson-Buck, A.; Su, X.; Giraldez, M. D.; Zhao, M.; Tewari, M.; Walter, N. G. Kinetic fingerprinting to identify and count single nucleic acids. *Nat. Biotechnol.* **2015**, *33*, 730−732.
(21) Steel, A. B.; Herne, A. T.; Tarlov, M. J. Electrochemical quantitation of DNA immobilized on gold. *Anal. Chem.* **1998**, *70*, 4670−4677.
(22) Huang, Y.; Zhang, Y. L.; Xu, X.; Jiang, J. H.; Shen, G. L.; Yu, R. Q. Highly specific and sensitive electrochemical genotyping via gap ligation reaction and surface hybridization detection. *J. Am. Chem. Soc.* **2009**, *131*, 2478−2480.
(23) Wang, J. Y.; Zhang, Y. J.; Li, H.; Hu, X. L.; Li, M. P.; Song, P. Y.; Ma, Q. L.; Peng, L. M.; Chen, X. P. CRISPLD1 rs12115090 polymorphisms alters antiplatelet potency of clopidogrel in coronary artery disease patients in chinese han. *Gene* **2018**, *678*, 226−232.
(24) Modrich, P. DNA mismatch correction. *Annu. Rev. Biochem.* **1987**, *56*, 435−466.
(25) Gao, X.; Geng, M.; Li, Y.; Wang, X.; Yu, H. Z. Revealing and resolving the restrained enzymatic cleavage of DNA self-assembled monolayers on gold: electrochemical quantitation and ESI-MS confirmation. *Anal. Chem.* **2017**, *89*, 2464−2471.
(26) Zhang, X.; Wang, F.; Liu, B.; Kelly, E. Y.; Servos, M. R.; Liu, J. Adsorption of DNA oligonucleotides by titanium dioxide nanoparticles. *Langmuir* **2014**, *30*, 839−845.

https://dx.doi.org/10.1021/acssensors.0c02720
ACS Sens. 2021, 6, 1348−1356